Unsteady Effect in a Nozzled Turbocharger Turbine

Srithar Rajoo
e-mail: srithar.rajoo@imperial.ac.uk

R. F. Martinez-Botas
Reader
e-mail: r.botas@imperial.ac.uk

Department of Mechanical Engineering,
Imperial College London,
South Kensington Campus,
London SW7 2AZ, UK

The unsteady behavior of a nozzled turbocharger turbine under pulsating flow conditions has been studied experimentally in a cold flow test facility that replicates engine pulses. The results presented are obtained at a turbine speed of 48,000 rpm for pulsating frequencies of 40 Hz and 60 Hz (which correspond to 1600 rpm and 2400 rpm in a twin turbocharger six cylinder internal combustion engine). The turbine unsteady behavior is compared for nozzle vane angles ranging between 40 deg and 70 deg. A nozzled turbocharger turbine is found to behave differently from a nozzleless turbine under pulsating flow. The existence of a nozzle ring "damps" the unsteady flow leading to a reduced level of flow dynamics affecting the turbine wheel for all vane angles. The bigger volume in the nozzled turbine is also another contributing factor to the observed characteristics. The results are more pronounced in the higher frequency and maximum vane opening condition. Given this "damping" behavior, the concept of unsteady efficiency is questioned. The level of unsteadiness in the flow is characterized by the relevant nondimensional parameters, and the onset of the unsteadiness in the flow and its effect on a nozzled turbocharger turbine is discussed. The onset of the unsteady effect is suggested to be at 40 Hz flow condition. However, the nozzled turbine exhibits more of filling and emptying characteristics for both the frequency conditions, especially at close nozzle position cases. The effect of unsteadiness on the instantaneous efficiency calculation is more pronounced in the nozzled turbine compared with a nozzleless turbine.
[DOI: 10.1115/1.3142862]

1 Introduction

Understanding turbine unsteady behavior is crucial in the design of turbochargers in order to further improve turbocharger/engine matching. It is common practice to select turbochargers based on steady-state assumptions, which in most cases does not include the unsteady characteristics. This paper aims to provide insights into the turbine's unsteady behavior by characterizing the level of unsteadiness in a turbocharger stage with a nozzled-mixed-flow turbine. Even though there has been considerable amount of studies on turbine unsteady performance, most of these investigations are based on nozzleless systems [1–5]. However, nozzled stages are ever more common due to the increasing use of variable geometry turbochargers (VGTs) that aim to improve turbocharger-response as well as to reduce emissions. The question of whether the unsteady concepts that apply to a nozzleless turbine are similar to a nozzled turbine remains yet to be answered.

2 Experimental Setup

An in-house developed mixed-flow turbine [6] is used in the current study with a purposely designed volute with pivoting nozzle vanes. The meridional view of the mixed-flow turbine and the nozzle vane assembly is shown in Fig. 1. A set of 15 vanes is coupled to a ring, which enables pivoting in the range of 40–70 deg (from the radial direction), corresponding to the fully opened 71% closure nozzle vane position, respectively.

Figure 2 shows the schematic of the turbocharger test-rig used in the current study. The test-rig is a cold flow facility where the turbine is fed with compressed air, heated sufficiently to avoid condensation at the turbine exit. The turbine is loaded through a high speed permanent magnet eddy-current dynamometer [7]. A pulse generator consisting of two counter-rotating chopper plates is used to create pulsation in the flow simulating a diesel engine exhaust stream in frequency and amplitude. Some of the important measuring instruments in the test facility are also shown in Fig. 2. The chopper plate rotation is measured with a shaft encoder, which directly reflects the flow frequency. A single transistor-transistor logic (TTL) signal per revolution of the encoder is used as a trigger mark in the software to simultaneously log all relevant instantaneous parameters. The air mass flow rate during steady testing is measured with an orifice plate upstream of the pulse generator.

The measuring plane in Fig. 2 is the position in the test-rig where the isentropic conditions of flow are measured in unsteady testing. A traversing hotwire is used to measure the flow velocities in 36 locations in the pipe cross section, which are then integrated and converted to the instantaneous mass flow rate with an in situ calibrated function. A fast response strain-gauge transducer is used to measure the instantaneous pressure of the flow. The average temperature of the flow is measured with an E-type thermocouple, which is then used with the instantaneous pressure to calculate the instantaneous temperature by isentropic relationship.

The instantaneous actual condition of the turbine is measured at the dynamometer end. An optical sensor is used to measure the instantaneous speed of the turbine, which is differentiated to obtain the rotor acceleration. The product of the rotor's acceleration and the rotating inertia is the fluctuating torque. The instantaneous torque of the turbine is the sum of the fluctuating and the average torque (measured with a load cell). The nozzle vane's angle is set and monitored through a linear voltage displacement transducer (LVDT). The LVDT is mechanically coupled to the nozzle vane ring and calibrated for the vane angle. A detailed discussion of all the instantaneous measurement and analysis is given in Ref. [5].

The unsteady test conditions are set up by using the steady-state velocity ratio as the operating point. In this manner, the time averaged operating point in an unsteady test is set to correspond approximately to its peak steady efficiency. The mean temperature of the flow is also held constant to the steady condition. The unsteady test is set to a constant nondimensional speed to the steady condition. Due to the arrangement of the chopper plate and

Contributed by the International Gas Turbine Institute of ASME for publication in the JOURNAL OF TURBOMACHINERY. Manuscript received July 25, 2007; final manuscript received August 28, 2008; published online March 24, 2010. Review conducted by David Wisler. Paper presented at the ASME Turbo Expo 2007: Land, Sea and Air (GT2008), Montreal, QC, Canada, May 14–17, 2007.

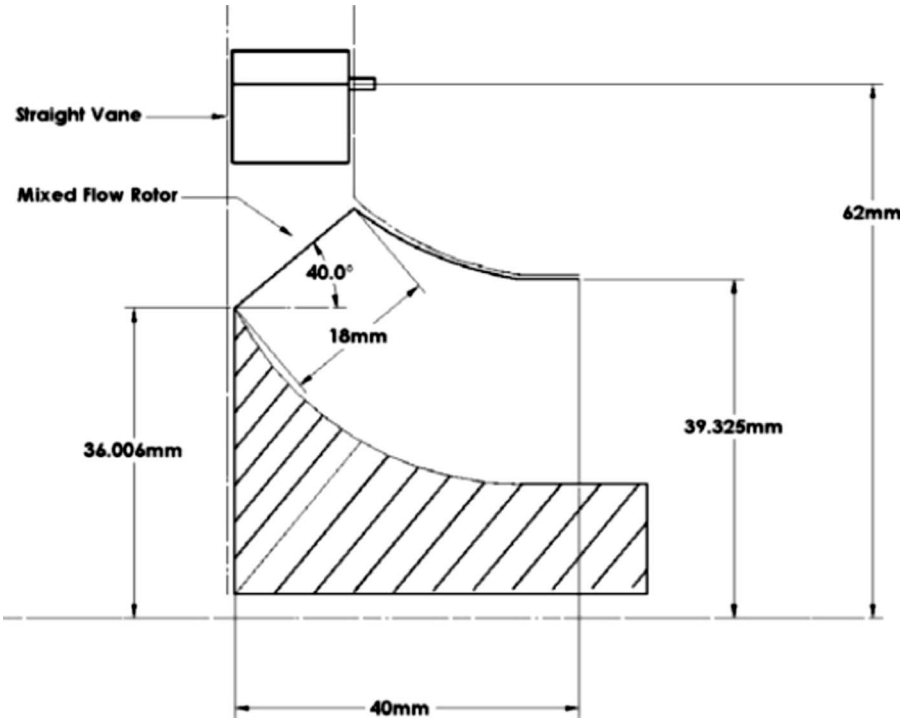

Fig. 1 Meridional view of the mixed-flow turbine and the nozzle vane used in the current study

the specific setup of the test conditions, the amplitude of the inlet pulse will reduce as the frequency increases for an equivalent rotor speed (Fig. 14). Thus, the discussion of the unsteady results in the current paper is within this limitation.

3 Results and Discussions

3.1 Steady-State Turbine Performance. The pivoting vane mixed-flow turbine is tested with steady flow over a range of velocity ratios (ranging from 0.5 to 1.1) at all vane positions for an equivalent speed of 80% (48,000 rpm). Figure 3 shows that the turbine efficiency increases from fully open vane condition (40 deg) until it reaches a peak of about 80% at a vane angle setting between 60 deg and 65 deg, and then decreases as the vanes close toward a 70 deg vane angle. The velocity ratio at the vane angle setting where the peak efficiency occurs is similar to the value obtained in a nozzleless arrangement of the same wheel. The velocity ratio for peak efficiency increases from 0.53 to 0.62 corresponding to vanes opening from 70 deg to 40 deg, respectively. The shift in the velocity ratio at the peak is due to the change in the flow condition at different vane angle settings. This can be explained in a simplified way with a velocity triangle at the rotor inlet, as shown in Fig. 4. The increase in the absolute flow angle (α) when the nozzle closes (toward 70 deg) will result in the increase in the loading factor (ψ) at fixed rotor tip speed (U). As the velocity ratio is inversely proportional to the loading factor, its value will tend to decrease but limited by generally higher efficiency at closer nozzle positions. However, noticeable decrease in the velocity ratio is observed at 70 deg compared with the other vane angle settings. This suggests that the high flow blockage at the nozzle entry increases the upstream pressure (see Fig. 14), contributing to the decrease in the velocity ratio. Figure 5 shows that the turbine's swallowing capacity increases as the vanes open up from 70 deg to 40 deg as might be expected. At a 40 deg vane angle setting, the swallowing capacity is approximately 50%

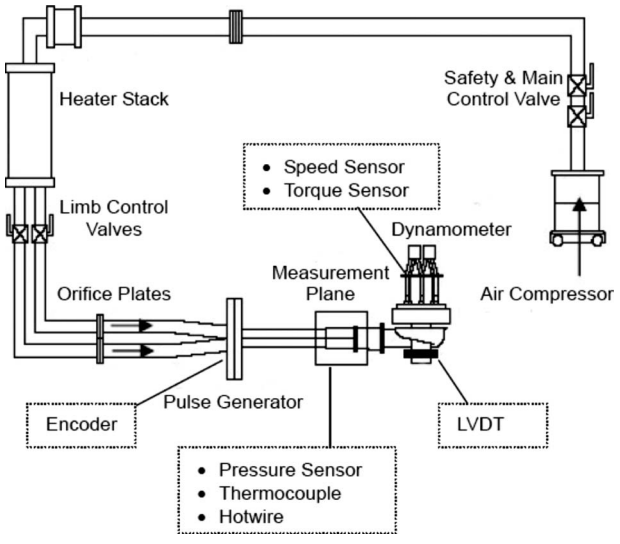

Fig. 2 Schematic of the turbocharger test facility and the measuring instruments

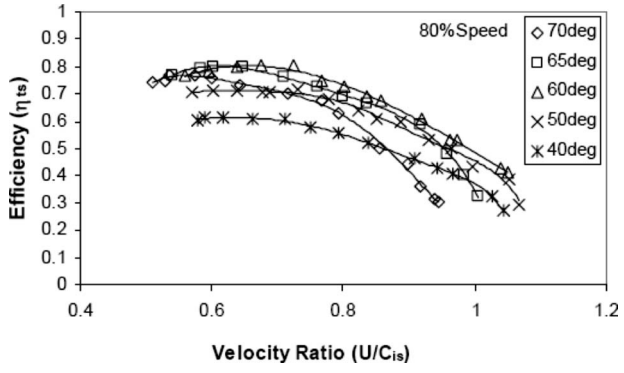

Fig. 3 Efficiency versus velocity ratio of the pivoting vane mixed-flow turbine

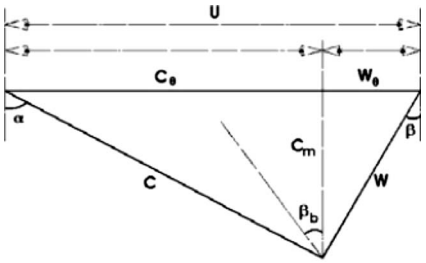

$$\frac{U}{C_{is}} \approx \frac{\eta}{\sqrt{2\psi}} = \frac{\eta}{\sqrt{2\dfrac{C_\theta}{U}}}$$

Fig. 4 Velocity triangle at the rotor inlet

higher than the 70 deg setting but the peak efficiency is 21% lower.

3.2 Effect of the Pulsating Flow Frequency. The effect of pulse frequencies (40 Hz and 60 Hz) on performance is shown in Fig. 6 for a 60 deg vane angle setting. The equivalent quasisteady curve is also superimposed in this figure. For both frequencies, the unsteady curve envelopes around the steady curve, which is explained by the continuous emptying and the filling of the large volume (pipe+volute) from the measuring plane to the rotor inlet. At 60 Hz condition, the unsteady curve shifts toward a lower pressure ratio compared with the 40 Hz condition. This is due to the shorter duty cycle at 60 Hz condition reducing mass accumulation in the piping and volute over 1 cycle period, compared with 40 Hz condition.

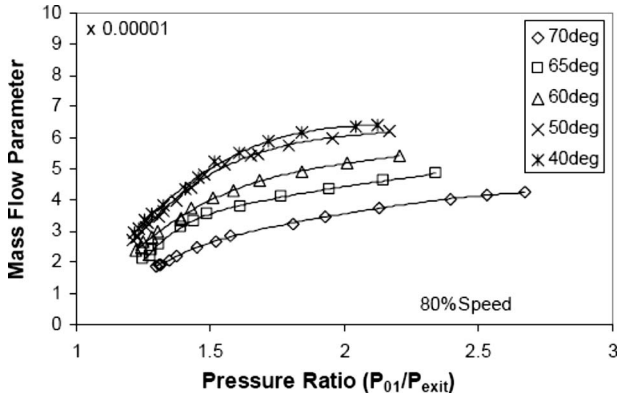

Fig. 5 Mass flow parameter versus pressure ratio of the pivoting vane mixed-flow turbine

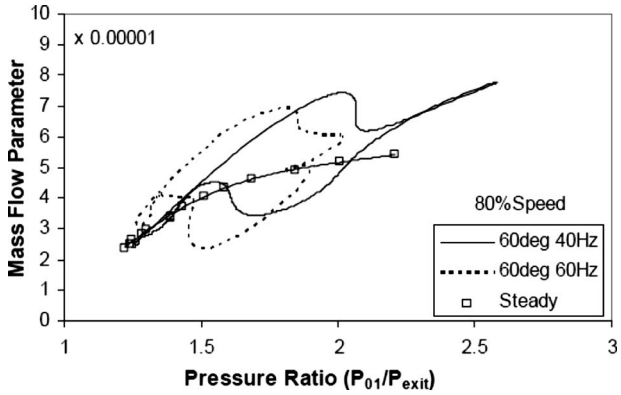

Fig. 6 Turbine's instantaneous swallowing capacity at 60 deg vane angle, with 40 Hz and 60 Hz pulsating flows

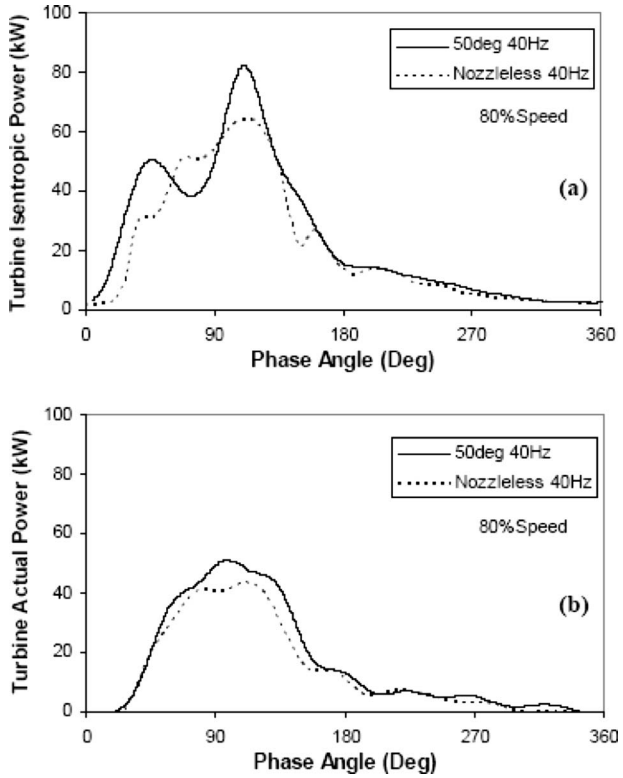

Fig. 7 Turbine's isentropic (*a*) and actual (*b*) power for 1 cycle of 40 Hz pulsating flow (nozzleless [8])

Figure 7 shows the isentropic and actual power for 1 cycle at 40 Hz pulsating frequency, and the similar curves for 60 Hz condition are given in Fig. 8. The result shown is for a 50 deg vane angle setting, where the turbine's steady swallowing capacity is

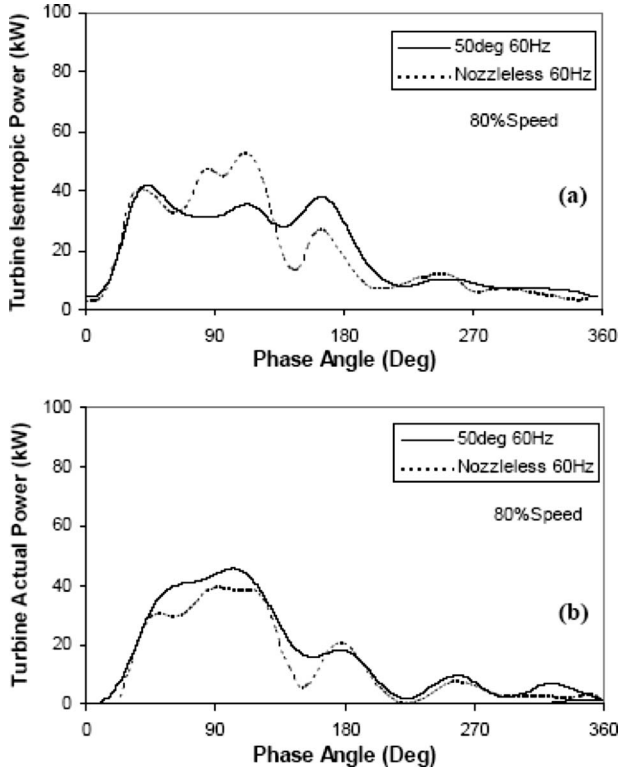

Fig. 8 Turbine's isentropic (*a*) and actual (*b*) power for 1 cycle of 60 Hz pulsating flow (nozzleless [8])

similar to the nozzleless unit. Note that the actual power is measured at the turbine shaft while the isentropic condition is measured at the measuring plane (see Fig. 2); thus, both these measurements are not in phase when compared instantaneously but in this case phase shifted with the sonic plus bulk flow velocity method [5]. The higher fluctuation in the isentropic power shows that the flow is more dynamic in the 60 Hz condition compared with the 40 Hz condition. On the other hand, the isentropic power in the 40 Hz condition exhibits a higher peak compared with a more flat fluctuation in the 60 Hz condition. This is because of the combinational effects of pressure wave reflections and the higher mass accumulation in the piping and the volute at 40 Hz condition, whereas the rate of mass emptying through the turbine is similar in both conditions (same vane opening and speed). These effects are found to be more significant in a nozzled turbine compared with a nozzleless turbine (see Figs. 7 and 8).

The actual power of the turbine is less affected by the flow frequency compared with the upstream isentropic power. The peak actual power is slightly lower at 60 Hz compared with the 40 Hz condition. The fluctuation in the isentropic power is not completely reflected in the actual power of the turbine in the nozzled turbine especially at the peak region. This is in contrast to a nozzleless turbine where the fluctuation in the isentropic condition affects the turbine actual power over the whole pulse region [8], as seen in Figs. 7 and 8. This suggests that the nozzle ring acts as a "damping body," which shields the turbine rotor from complete exposure to the unsteadiness in the flow upstream. Furthermore, the bigger volume in the nozzled stator (48% bigger) contributes to the increase in the filling/emptying effect. However, the existence of a nozzle ring creates an intermediate volume, which has different filling/emptying characteristics compared with the upstream volume (pipe+volute). It is suggested that the combinational effect of the increase in volume and the intermediate body contributes to the difference in the characteristics observed in the nozzled turbine. Based on the current test configuration, no conclusive statement can be made on these effects individually. The use of 1D and 3D-CFD will be profitable in characterizing these phenomena.

3.3 Effect of the Nozzle Vane Angle. The turbine is tested at different nozzle vane angle settings, ranging from an almost closed position of 70 deg to fully open position of 40 deg. Figures 9 and 10 show the turbine instantaneous swallowing capacity at different vane angle settings for both 40 Hz and 60 Hz conditions, respectively. The equivalent curve with quasisteady approach is also given for individual test cases. The pressure ratios experienced by the turbine over an unsteady cycle reduce as the nozzle vanes open from 70 deg to 40 deg. The more open position of the nozzle vanes leads to a greater degree of mass emptying and lower back pressure. The shift in the pressure ratios is more significant at 40 Hz condition than at the 60 Hz condition. Another related observation is that the turbine experiences a period of choking at closer vane positions (especially 70 deg), which is more significant during 40 Hz condition. This is reflected in the hysteresis loop of the unsteady curve at close nozzle positions, where it shifts higher than the equivalent quasisteady curve. The range of the mass flow parameter of the turbine over an unsteady cycle is similar in all vane angle settings at 40 Hz condition, but at 60 Hz condition the range reduces as the nozzle vanes open to 40 deg.

Figure 11 shows the changes in the isentropic (a) and actual (b) power from a closer vane position (70 deg) to a fully open vane position (40 deg) at 40 Hz condition. Similar results at 60 Hz condition are shown in Fig. 12. The isentropic power shows a higher level of unsteadiness with more localized fluctuations at 40 deg vane angle position. This suggests a higher level of pressure wave reflections at a more open vane position. The choking of the turbine is also reflected in the higher peak of the isentropic power at 70 deg vane angle position, especially at 40 Hz condition. The choking of the turbine at 70 deg vane angle position results in the peak actual power to be lower than at the 40 deg vane angle position. However, at the lower region of the pulse, the closer vane position obviously increases the momentum impact on the rotor and results in a higher actual turbine power. The changes in the actual power are observed to not completely follow the fluctuation in the isentropic power, regardless of the vane angle positions. The level at which the turbine's actual power follows the fluctuation in the isentropic power is more dependent on the pulsating flow frequency than the nozzle vane angle positions.

Figure 13 shows the cycle averaged velocity ratio of the turbine at different vane angles for 40 Hz and 60 Hz pulsating flow con-

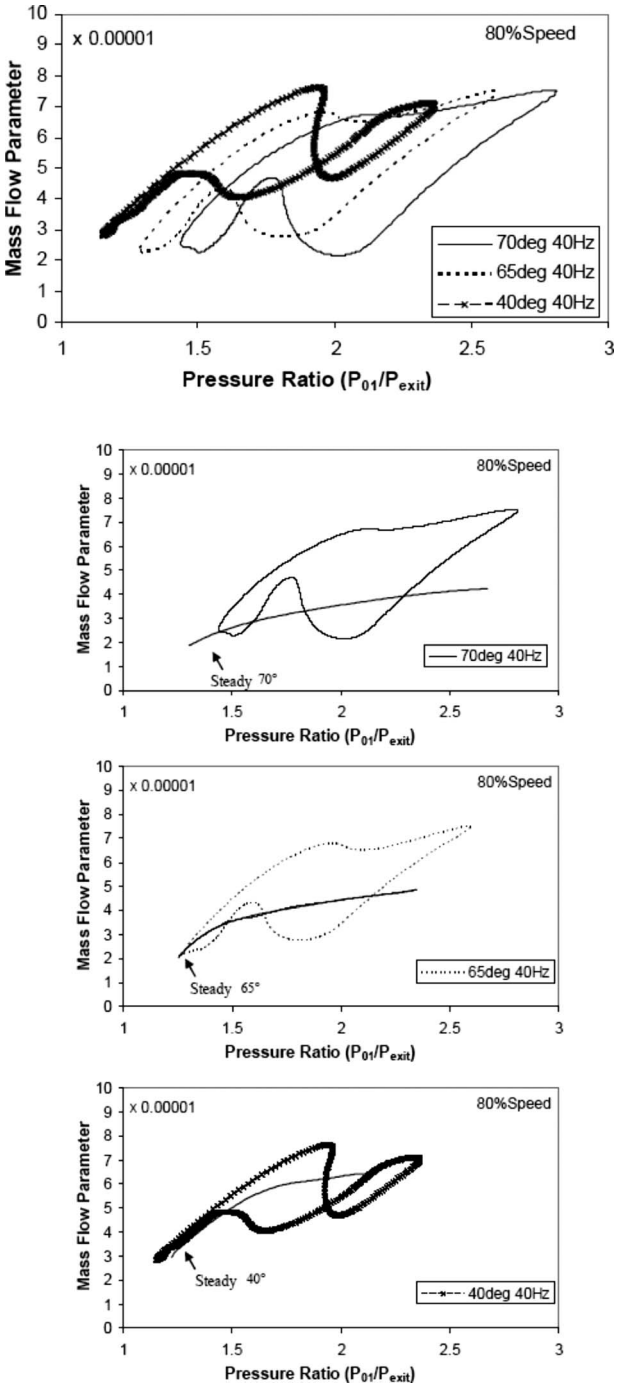

Fig. 9 Turbine's instantaneous swallowing capacity for different vane angles at 40 Hz pulsating flow

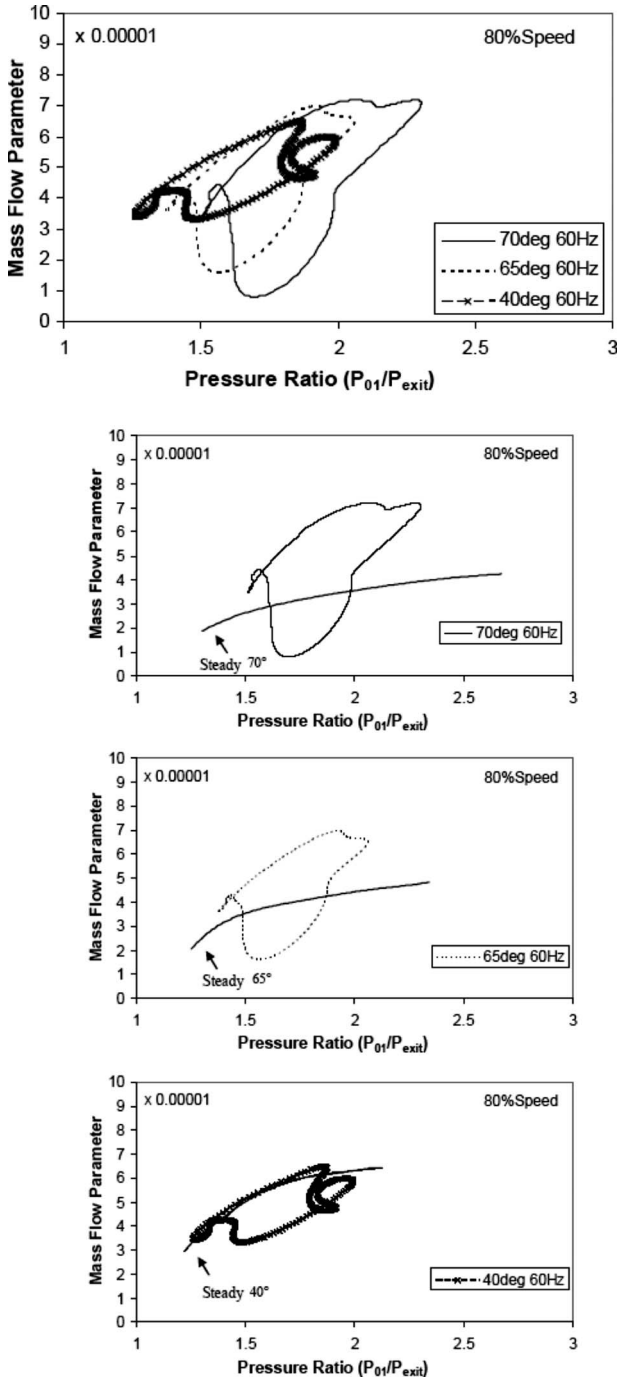

Fig. 10 Turbine's instantaneous swallowing capacity for different vane angles at 60 Hz pulsating flow

ditions. The cycle averaged value is calculated by isentropic power averaging method, Eq. (1), as proposed by Szymko et al. [5].

$$\left(\frac{U}{C_{is}}\right)_{cyc\_avg} = \frac{\int_0^{\theta}\left[\frac{U}{C_{is}}(t)\cdot \dot{W}(t)_{is}\right]dt}{\int_0^{\theta}\dot{W}(t)_{is}dt} \quad (1)$$

The cycle averaged velocity ratio shows a downward trend as the nozzle vane changes to closer positions. The change is small from 40 deg to 60 deg vane angle positions but beyond that the velocity

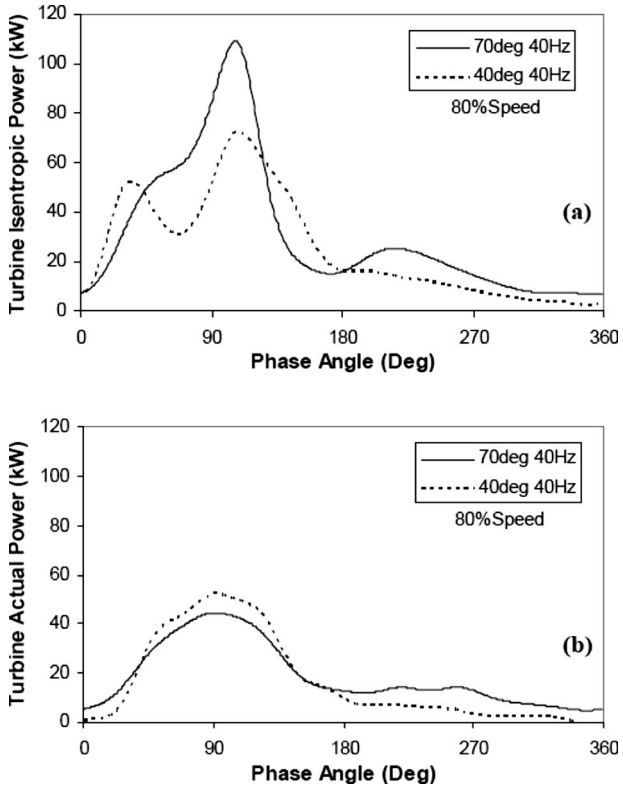

Fig. 11 Turbine's isentropic (*a*) and actual (*b*) power for a 40 Hz pulsating cycle at different vane angles

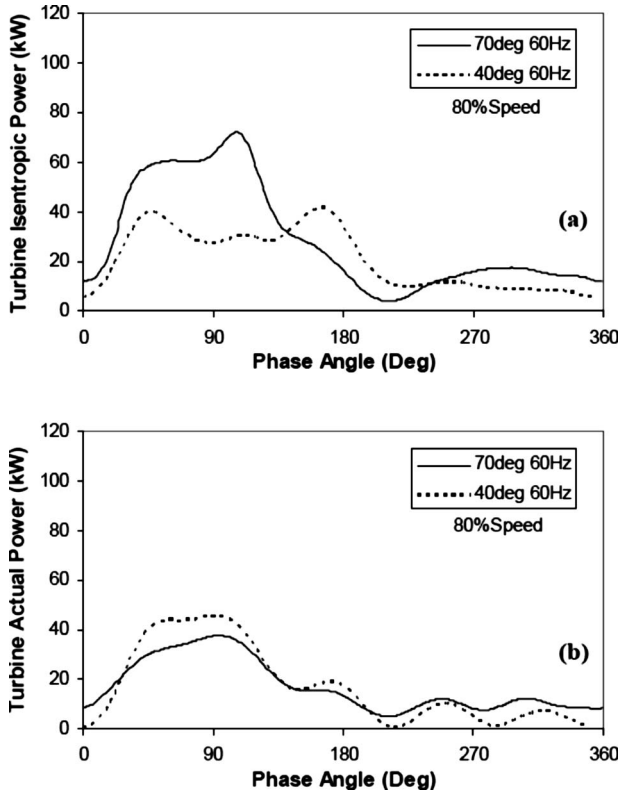

Fig. 12 Turbine's isentropic (*a*) and actual (*b*) power for a 60 Hz pulsating cycle at different vane angles

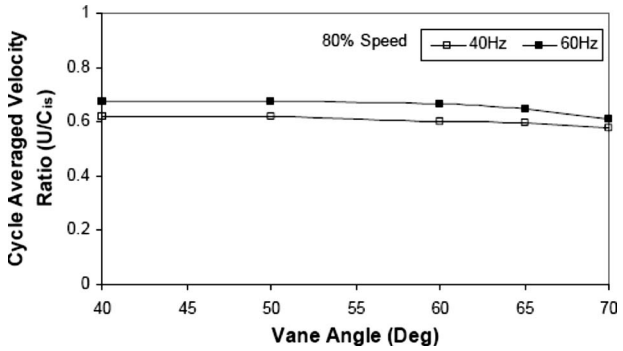

Fig. 13 Cycle averaged velocity ratio (U/C_{is}) at different vane angles

ratio decreases at a higher rate. Since the rotor speed is similar in all the cases, the variation in velocity ratio is mainly due to the instantaneous expansion ratio changes. The pressure traces in Fig. 14 could also be used to show the decrease in the velocity ratio at close nozzle positions, especially at 70 deg.

3.4 Instantaneous Efficiency. In an unsteady testing, the isentropic and actual conditions of the turbine are measured instantaneously at two different locations (Fig. 2). This has to be the case for a radial or mixed-flow turbine with a volute because the rotor accepts energy around the periphery of the volute exit and a unique location of isentropic energy does not exist (distinct from an axial turbomachine). The difference in the measuring location creates a phase difference and in effect produces two separate parameters, which need to be linked to deduce the efficiency. The phase shifting methods, which have been proposed and used, are sonic velocity method [1], bulk flow method [3,9], and sonic plus bulk flow method [5]. The difference between these methods is in

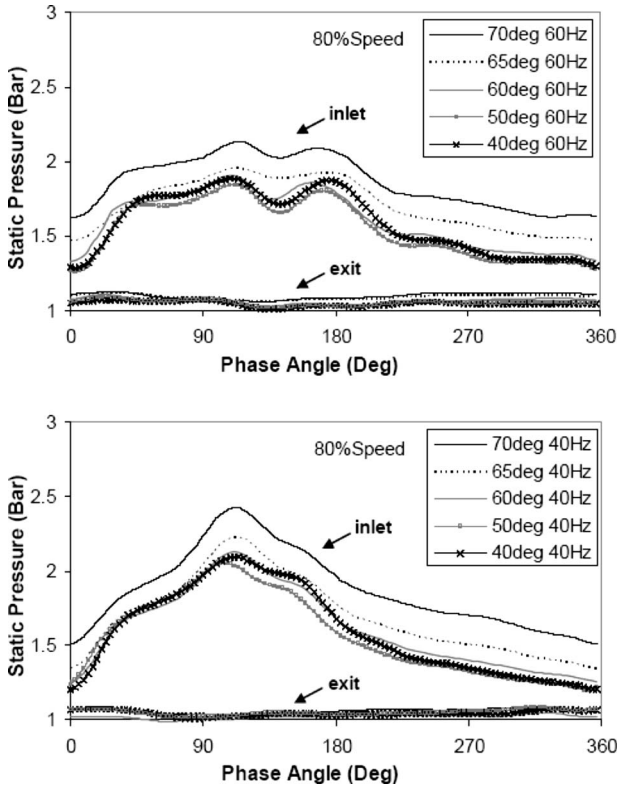

Fig. 14 Measured instantaneous inlet static pressure at different vane angles

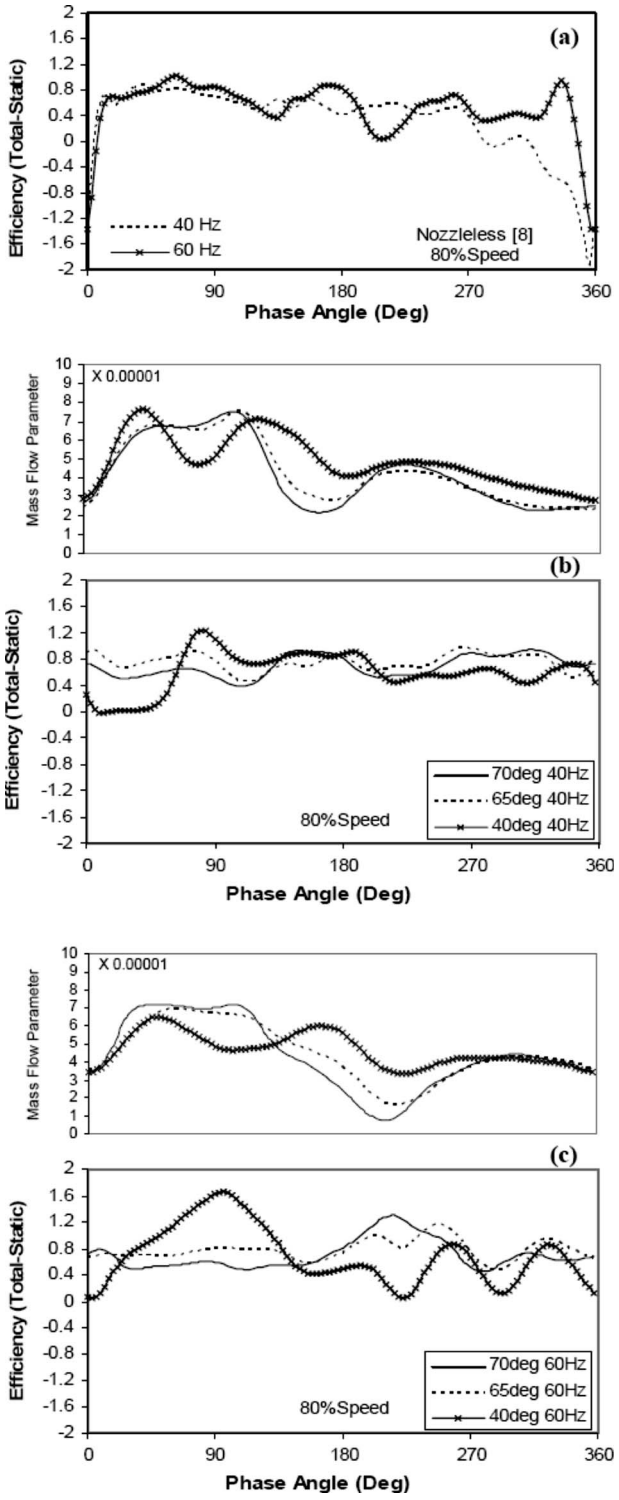

Fig. 15 Instantaneous efficiency of a nozzleless turbine (*a*) [8] and nozzled turbine with different vane angle settings at 40 Hz (*b*) and 60 Hz (*c*) pulsating flows

the pulse traveling velocity assumption. Thus the instantaneous efficiency calculation on a point-by-point comparison depends heavily on the shifting method and thus may be misleading when thinking about the instantaneous performance of the turbine. Nevertheless to illustrate the point, Fig. 15 shows the instantaneous efficiency calculated with point-by-point comparison of the actual and isentropic condition after the sonic plus bulk flow speed phase shift. Efficiency curves for a nozzleless turbine at different flow

Table 1 Cycle average (energy weighted) and quasisteady efficiency at different vane angles

Vane angle (deg)	U/C_{is}	Cycle average efficiency	Quasisteady efficiency
		40 Hz	
70	0.578	0.599	0.736
65	0.598	0.697	0.756
60	0.599	0.646	0.759
50	0.619	0.649	0.669
40	0.621	0.658	0.574
		60 Hz	
70	0.608	0.594	0.744
65	0.648	0.746	0.770
60	0.665	0.776	0.765
50	0.675	0.835	0.683
40	0.674	0.822	0.585

frequencies are given in Fig. 15(*a*), and the similar curves for a nozzled turbine with different vane angle settings are shown in Figs. 15(*b*) and 15(*c*) (instantaneous mass flow parameter is given for reference). The value of instantaneous efficiency goes higher than unity in all cases and it further increases with frequency. It appears, however, that phase shifting and its inaccuracy affect the evaluation of unsteady efficiency much more in the case of a nozzled system than one without nozzles.

In reality it is thermodynamically unreasonable to suggest efficiencies greater than unity, and the authors are not suggesting otherwise. Figure 15 simply illustrates the void in the current unsteady methodology to accurately assess a radial/mixed-flow turbine instantaneous efficiency with the aim of achieving satisfactory design criterion for a turbocharger. One solution for this is to compare the cycle averaged power to deduce the cycle averaged efficiency. Such efficiency exhibits the behavior of the turbine over a pulse cycle but naturally lacks instantaneous features. The cycle averaged efficiency and the estimated equivalent quasisteady value for different test conditions are given in Table 1. In each instance of time in an unsteady cycle, the measured instantaneous velocity ratio is used to extract the equivalent quasisteady efficiency from the steady map. These quasisteady efficiencies are then averaged using the isentropic power averaging method [5] to obtain the cycle averaged quasisteady efficiency. Figure 16 shows the cycle averaged power with different vane angle settings at 40 Hz and 60 Hz pulsating flows. The cycle averaged actual power of the turbine is almost similar at all vane angle settings and frequencies. But the cycle averaged isentropic power shows a greater difference especially at closer vane angle settings due to the nozzle choking, which is also reflected in the decrease in the velocity ratio (see Fig. 13). The cycle averaged efficiency of the turbine is found to be generally higher at 60 Hz flow condition compared with the 40 Hz condition. The variation in the cycle averaged efficiency over the vane angle range at 40 Hz flow shows similarity to the quasisteady value, with the peak at 60 deg/65 deg settings and lower efficiency as the vane angle moves to either open or close. However, this is not the case at 60 Hz flow condition, where the more open vane positions exhibit higher cycle averaged efficiencies compared with the close vane position. The cycle averaged efficiencies at 60 Hz-40 deg and 60 Hz-70 deg conditions are 82% and 60%, respectively. This is completely different from the quasisteady efficiencies (Table 1), which are 58% (40 deg) and 74% (70 deg). For the vane angle setting of 60 deg/65deg (peak steady efficiency settings), the cycle averaged efficiency is closer to the equivalent quasisteady value in the 60 Hz conditions. The same could not be said for the 40 Hz condition, even though the comparison is better than the fully open/closed nozzle settings. In the authors' opinion the cycle averaged efficiency is not the optimum solution in an unsteady methodology especially for nozzled turbine, even though it should be noted that it is satisfactorily used in many cases. Thus more study and analysis need to be carried out especially with 1D and 3D-CFD methods to formulate a better way of defining a nozzled radial/mixed-flow instantaneous efficiency in an unsteady cycle.

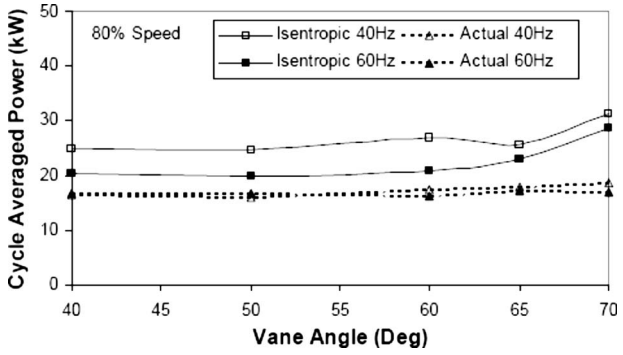

Fig. 16 Cycle averaged turbine power with different vane angle settings at 40 Hz and 60 Hz pulsating flows

3.5 Unsteadiness Parameter. The Strouhal number, St, is usually used as the basis for measuring the effects of unsteady flow in fluid machinery, Eq. (2).

$$\mathrm{St} = \frac{fd}{v} \tag{2}$$

A modified version of Eq. (2) is the reduced frequency, β [10], as given in Eq. (3).

$$\beta = \frac{\omega L}{v} \tag{3}$$

The importance of the unsteady effect can be assessed by using the reduced frequency as a criterion [5,10,11], where if $\beta \ll 1$, unsteady effects are small; if $\beta \gg 1$, unsteady effects dominate; and if $b \approx 1$, both steady and unsteady effects are important.

Since the pulse waveform in a turbocharger is not sinusoidal, further modifications are proposed [5], which take into account the pulse fraction over a period. Modified Strouhal number, MSt, is given in Eq. (4).

$$\mathrm{MSt} = \frac{fL}{v} \cdot \frac{1}{2\phi} \tag{4}$$

If the gas velocity, v, in Eq. (4) is replaced with the velocity at which pressure waves are propagated, one arrives at the pressure-modified Strouhal number, PMSt, as in Eq. (5).

$$\mathrm{PMSt} = \frac{fL}{v \pm a} \cdot \frac{1}{2\phi} \tag{5}$$

Based on MSt and PMSt values, the turbine unsteady condition can be described as quasisteady ($\mathrm{MSt} < 0.1$), steady encapsulated hysteresis ($\mathrm{PMSt} < 0.1$), or fully unsteady ($\mathrm{PMSt} > 0.1$). Table 2 shows the unsteadiness parameter values (Eqs. (2)–(5)) for different vane angle positions at 40 Hz and 60 Hz pulsating flow conditions. The length scale, L, used is 0.79 m, which is the distance from the measuring plane to the 180 deg azimuth angle location in the volute. The values of the unsteadiness parameter show a very minimal change over the different vane angle positions for both flow frequency conditions. The values suggest the beginning of the onset of unsteady effect at 40 Hz flow condition, with the closer vane position slightly more unsteady. At 60 Hz flow conditions, the higher than 0.1 values for both the MSt and PMSt suggest a full unsteady regime. However, comparison between

Table 2 Unsteadiness parameters for nozzle vane angle range of 40–70 deg, pulse frequencies of 40 Hz and 60 Hz, length scale of 0.79 m, and $\phi=\frac{1}{3}$

Vane angle (deg)	St	β	MSt	PMSt
		40 Hz		
70	0.316	1.987	0.474	0.101
65	0.314	1.971	0.470	0.102
60	0.283	1.780	0.425	0.099
50	0.277	1.740	0.416	0.099
40	0.274	1.724	0.412	0.099
		60 Hz		
70	0.465	2.921	0.697	0.151
65	0.458	2.877	0.687	0.150
60	0.451	2.832	0.676	0.151
50	0.433	2.718	0.649	0.150
40	0.448	2.817	0.672	0.151

unsteady and quasisteady curves shows that the turbine exhibits more of filling and emptying characteristics for both the frequency conditions, especially at close nozzle position cases. This can be due to the larger volume in the nozzled turbine (~48% bigger volume). Additionally, this could also be due to the lower swallowing capacity of the nozzled turbine (at closed position), which leads to mass accumulation and possible choking. Thus, the thresholds of the unsteadiness parameters need to be defined with more experimental results, and additional computational analysis will be profitable.

4 Conclusions

The current paper investigates the unsteady behavior of a nozzled turbocharger turbine in comparison to a nozzleless version. The turbine is based on a mixed-flow rotor for which a pivoting nozzle vane stator is designed with a vane angle range of 40–70 deg.

The existence of a nozzle vane ring is found to act as a damping body that shields the turbine rotor from the upstream flow fluctuation. This is more significant at higher flow frequency and at a more open vane positions. Furthermore, the increase in the volume of nozzled volute compared with the nozzleless unit could also contribute to the difference in turbine characteristics observed.

The turbine observed goes through choking in a pulse cycle at closer vane position because of the faster rate of mass accumulation in the piping and volute compared with the emptying rate through the turbine. The choking is more significant at 40 Hz condition compared with 60 Hz.

The point-by-point calculation of instantaneous turbine efficiency in an unsteady cycle is deemed to be inaccurate especially at higher frequency condition. This is because of the difference in the location of actual and isentropic condition measurement. The discrepancies in the instantaneous efficiency are more critical in a nozzled turbine because of the nozzle ring affecting the unsteady features of the pulsating flow before it imparts energy to the rotor.

The use of reduced frequency analysis in the form of relevant parameters, St, β, MSt, and PMSt, is discussed. The frequency of the pulsating flow is found to be the dominant parameter in deciding the onset of the full unsteady regime. The values of unsteadiness parameters are found to be very similar over a range of vane angle settings. At 40 Hz condition the PMSt value is about 0.1 in all vane angle settings, whereby at 60 Hz it is about 0.15. The level of unsteadiness based on these PMSt values shows similarity to a nozzleless turbine, but the unsteady effect on the performance is found to be more significant in a nozzled turbine.

Acknowledgment

The authors would like to thank the Engineering and Physical Sciences Research Council (EPSRC) and University Technology Malaysia for their financial support and Holset Engineering, Mr. Harminder Flora, and Mr. John Laker for their strong technical support.

Nomenclature

a = speed of sound, m s^{-1}
C = absolute flow velocity, m s^{-1}
CFD = computational fluid dynamics
C_{is} = isentropic expansion velocity, m s^{-1}
d = cylinder diameter, characteristic length of flow, m
f = Karman vortex sheet frequency, wave frequency
L = characteristic length scale, m
mass flow parameter = $\dot{m}(T_{01})^{0.5}/p_{01}$
MSt = modified Strouhal number
p, P = pressure, Pa
PMSt = pressure-modified Strouhal number
PR = pressure ratio, p_1/p_2
St = Strouhal number
T = temperature, K
U = rotor tip speed, m s^{-1}
v = gas velocity, m s^{-1}
W = relative flow velocity, m s^{-1}
$\dot{W}$ = turbine work, W
EGR = exhaust gas recirculation
rpm = revolution per minute

Subscripts

0 = total condition
1 = stage inlet
2 = stage exit
m = meridional direction
θ = tangential direction
cyc-avg = cycle averaged (isentropic power average method)

Greek letters

β = reduced frequency, $\omega L/v$
β = relative flow angle, deg
β_b = inlet blade angle, deg
α = absolute flow angle, deg
θ = air pulse period, s
ϕ = pulse length as a fraction of wavelength (duty cycle)
ω = angular frequency, $2\pi f$
ψ = loading coefficient
η = efficiency

References

[1] Dale, A., and Watson, N., 1986, "Vaneless Radial Turbine Performance," 3rd Int. Conf. of Turbocharging and Turbochargers, Proc. Inst. Mech. Eng., Paper No. C110/86, pp. 65–76.
[2] Winterbone, D. E., Nikpour, B., and Alexander, G. I., 1990, "Measurement of the Performance of a Radial Inflow Turbine in Steady and Unsteady Flow," 4th Int. Conf. of Turbocharging and Turbochargers, Proc. Inst. Mech. Eng., Paper No. C405/015, pp. 153–162.
[3] Baines, N. C., Hajilouy-Benisi, A., and Yeo, J. H., 1994, "The Pulse Flow Performance and Modelling of Radial Inflow Turbines," 5th Int. Conf. of Turbocharging and Turbochargers, Proc. Inst. Mech. Eng., Paper No. C484/006/94, pp. 209–219.
[4] Arcoumanis, C., Hakeem, I., Khezzar, L. and Martinez-Botas, R. F., 1995,

"Performance of a Mixed Flow Turbocharger Turbine Under Pulsating Flow Conditions," ASME Paper No. 95-GT-210.
[5] Szymko, S., Martinez-Botas, R. F., and Pullen, K. R., 2005, "Experimental Evaluation of Turbocharger Turbine Performance Under Pulsating Flow Conditions," ASME Paper No. GT 2005-68878.
[6] Abidat, M., Chen, H., and Baines, N. C., 1992, "Design of a Highly Loaded Mixed Flow Turbine," Proc. Inst. Mech. Eng., Part A, **206**, 95–107.
[7] Szymko, S., Martinez-Botas, R. F., Pullen, K. R., McGlashan, N. R., and Chen, H. A., 2002, "High-Speed, Permanent Magnet Eddy-Current Dynamometer for Turbocharger Research," 7th and 5th Int. Conf. of Turbocharging and Turbochargers, Proc. Inst. Mech. Eng., Paper No. C602-026, pp. 213–224.
[8] Szymko, S., 2006 "The Development of an Eddy Current Dynamometer for Evaluation of Steady and Pulsating Turbocharger Turbine Performance," Ph.D. thesis, Imperial College London, London, UK.
[9] Winterbone, D. E., Nikpour, B., and Frost, H., 1991, "A Contribution to the Understanding of Turbochargers Turbine Performance in Pulsating Flow," Internal Combustion Engine Research in Universities, Polytechnics and Colleges Conf., Proc. Inst. Mech. Eng., Paper No. C433/011, pp. 19–29.
[10] Greitzer, E. M., Tan, C. S., and Graf, M. B., 2004, *Internal Flow: Concepts and Applications*, Cambridge University Press, Cambridge, UK.
[11] Costall, A., Szymko, S., Martinez-Botas, R. F., Filsinger, D., and Ninkovic, D., 2006, "Assessment of Unsteady Behavior in Turbocharger Turbines," ASME Paper No. GT 2006-90348.